
IMPLICIT NEURAL REPRESENTATION OF TILEABLE MATERIAL TEXTURES

Hallison Paz
IMPA
hallpaz@impa.br

Tiago Novello
IMPA
tiago.novello@impa.br

Luiz Velho
IMPA
lvelho@impa.br

ABSTRACT

We explore sinusoidal neural networks to represent periodic tileable textures. Our approach leverages the Fourier series by initializing the first layer of a sinusoidal neural network with integer frequencies with a period P . We prove that the compositions of sinusoidal layers generate only integer frequencies with period P . As a result, our network learns a continuous representation of a periodic pattern, enabling direct evaluation at any spatial coordinate without the need for interpolation. To enforce the resulting pattern to be tileable, we add a regularization term, based on the Poisson equation, to the loss function. Our proposed neural implicit representation is compact and enables efficient reconstruction of high-resolution textures with high visual fidelity and sharpness across multiple levels of detail. We present applications of our approach in the domain of anti-aliased surface.

Keywords Implicit Neural Representation · Seamless Material · Sinusoidal Neural Networks

1 Introduction

Textures play a fundamental role in computer graphics, enabling the creation of visually appealing and realistic virtual environments. They model essential information of the surface materials in virtual scenes, enriching the visual experience with patterns that would be difficult to model otherwise. Within this scope, *periodic textures* stand out as an important example that models repeating patterns. They are used to represent materials found in domains such as architecture, textiles, and industrial design. Capturing the essence of such textures is an important task to bridge the gap between virtual scenes and their real-world counterparts.

Traditionally, texture tiles are depicted as discrete digital images. Discrete representations introduce potential challenges in sampling and interpolation for operations. This is particularly important for achieving seamless transitions.

Recently, *implicit neural representations* (INRs) have emerged as an alternative representation for images. They are a class of neural networks that take the 2D coordinates as input and output the continuous colors. INRs are continuous, compact, fast to evaluate, and have high representation capacity. Inspired by these properties, we propose to use INRs to represent seamless periodic textures. We focus on the subclass that uses the *sine* as activation function – *sinusoidal INRs* Sitzmann et al. [2020].

Training a sinusoidal INR to fit a given texture sample has the drawback of its image possibly being non-tileable. To avoid this, we introduce a condition for an INR to be *periodic* and propose a regularization term based on the *Poisson equation*. Regarding the periodicity of an INR, we observe that if one takes the first layer of a sinusoidal INR and initializes it with integer frequencies with a period P , the entire INR will be periodic with period P . This is due to the fact that the composition of sinusoidal layers expands as a sum of sines with frequencies given by integer combinations of the input layer, and the result is similarly periodic Novello [2022], Yüce et al. [2022]. We leverage this property to fit periodic signals such as image and texture representations.

The next step in our method involves defining a regularization term to ensure that the image produced by a periodic INR forms a seamless, tileable texture – meaning it should tile across the plane without displaying noticeable seams or discontinuities at the tile boundary. To achieve this, we employ the Poisson equation which enforces the INR gradient matches the original gradient within the domain (Poisson equation) and asks the INR to be equal to an image average on the domain border (periodic boundary values) Pérez et al. [2003]. It is important to note that for this problem to be well-posed, the boundary must be closed. However, since our network is periodic, we are solving the Poisson problem on the torus which allows us to also require gradient matching on the domain boundary (see the results in Section 4.3).

Besides the periodic representation, our method leads to better representation quality of images with fewer parameters in the architecture. Additionally, based on Fourier series, we design a frequency initialization that greatly decreases the amount of possible choices for frequencies. Our experiments demonstrate that this representation is suitable for representing periodic textures (and making them seamless) and can be easily integrated to the graphics pipeline for texture mapping. In summary, our contributions are:

- We propose an initialization scheme for sinusoidal INRs that uses integer multiples of a period P with reduced redundancy. We prove that this approach yields periodic INRs by demonstrating that the composition of periodic sinusoidal layers with period P preserves periodicity.
- To ensure seamlessness at the boundary domain, we introduce a regularization term based on the Poisson equation. We show that the resulting loss function can train a periodic INR to represent high-resolution textures with good quality and a reduced number of parameters. Moreover, these networks capture *sharp* details in the data.
- The proposed periodic INR framework showcases the ability to learn from specific segments of the ground-truth pattern without compromising information integrity.
- We apply our method in texture mapping, showcasing its versatility across texture representation tasks, such as multiresolution Paz et al. [2023].

2 Background and related methods

The scope of this work is to represent seamless material textures using *implicit neural representations* (INRs). Thus, it aims to encode the material texture of a surface through a periodic neural network $f : \mathbb{R}^2 \rightarrow \mathcal{C}$, where \mathcal{C} is the RGB color space, that can be trained based on data samples. More generally, it could be extended to the other channels of a material definition.

In this sense, the context is texture creation methods (procedural-based, capture-based, AI-based, and manual) with the purpose of being applied to a 3D surface by a rendering system.

Generating high-quality textured materials is challenging as they need to be visually realistic, seamlessly tileable, and have a small impact on the memory consumption of the application. For this reason, these materials are often created manually by skilled artists. In this work, we show that INRs can be used in those tasks.

Additionally, it is desirable to have an agnostic material representation based industry standards that is compatible with most rendering systems. One case is the Substance 3D Sampler from Adobe [2023], a creation platform of material collections that includes many tools for that very purpose. Next, we discuss the most relevant works that are related to our method.

2.1 Texture representations

Texture is ubiquitous in computer graphics. It is the key to represent visual information for the synthesis of naturalistic textures and images from photographic exemplars. Texture synthesis has grown into a mature field encompassing a variety of methods, such as: classic texture mapping Blinn and Newell [1976], procedural textures Perlin [1985], synthesis-by-example Efros and Leung [1999], and user-guided texture generation Haeberli [1990].

Wie et al. [2009] gives an overview of example-based texture synthesis methods. Also, Lagae et al. [2010] provides an in-depth account of noise primitives for procedural texturing. Recently, Yuksel et al. [2019] discusses alternative texture-mapping methods.

Most of the above methods target general texture patterns, however, there is a trend that investigates models of specific materials. This approach has the benefit of producing higher fidelity results by exploiting characteristics of important materials, such as wood. Jagnow et al. [2004] studies aggregate materials that are common in nature and formed by small particles.

2.2 Tileable Textures

While there is a large body of research devoted to texture mapping, little work, however, has been dedicated to synthesizing seamless tileable textures, which are important for the creation of materials. These textures have the property that when laid out in a regular grid of tiles form a homogeneous appearance suitable for use in memory-sensitive real-time graphics.

Lagae et al. [2008] gives an overview of tile-based methods in computer graphics applications. Additionally, we highlight the following methods. Wei [2004] presents a tile-based texture mapping algorithm that generates an arbitrarily large and non-periodic virtual texture map from the small set of stored texture tiles. Moritz et al. [2017] developed an approach to synthesize tileable textures using the PatchMatch texture synthesis algorithm. These methods rely on a particular algorithm that must be incorporated into the rendering system. Our INR representation, once trained is exported to be evaluated on the graphics hardware or, alternatively, can be used to generate a material tile.

Pérez et al. [2003] modeled the problem of making a rectangular domain texture tileable using a Poisson solver: the boundary conditions consist of forcing the opposite sides of the domain to be equals. In the interior, they asked for the gradient of the desired texture to be equal the ground-truth gradient. This approach works only on pixel-based images. Our method allows for the definition of a regularization term that compels the training of a periodic INR to produce a seamless, tileable texture. Furthermore, we can interchange the boundary and interior equations, given that our problem is defined on the 2D torus once the network is periodic.

2.3 Neural Textures

Texture representations strive to combine procedural methods with the fitting of data samples. The main trade-off is between computation and memory. Principled solutions to such issue come from *wavelets* and *neural networks*: Bajaj et al. [2000] addresses the memory problem by encoding 3D textures using a wavelet-based method, Gutierrez et al. [2019] describes a generative deep learning framework for 3D texture synthesis based on style transfer with results that are equivalent to patch based approaches.

Concerning tileable textures, Toulatzis and Fudos [2021] proposes an example-based texture synthesis using a deep learning process for creating tiles of arbitrary resolutions that resemble the structural components of an input texture. Zhou et al. [2022] developed a variant of StyleGAN whose architecture is modified to produce periodic material maps. These works employ "data-based neural networks" and generative models, conversely, our method uses "coord-based neural networks" and a representational spectral model.

Finally, Vaidyanathan et al. [2023] developed a neural compression technique specifically designed for material textures. Shi et al. [2020] introduced a deep neural feature-based graph creation method for constructing procedural materials. In this respect, our INR model is compact and can be incorporated into a neural rendering pipeline.

2.4 Implicit neural representations

Previous works such as Park et al. [2019], Mescheder et al. [2019], Sitzmann et al. [2020], Novello et al. [2022, 2023], da Silva et al. [2022], Yariv et al. [2020] demonstrated how to represent and render surfaces as level sets of neural networks. Due to the spectral bias inherent in *multilayer perceptrons* (MLPs) Rahaman et al. [2018], coordinate-based architectures often employ techniques like Fourier Feature Mapping Tancik et al. [2020] to map inputs to higher-dimensional spaces. Sinusoidal networks offer an alternative solution by utilizing periodic activation functions and operating on the spectral representation of the signal. However, the composition of sinusoidal layers can introduce new frequencies, making it challenging to train deep sinusoidal neural networks Parascandolo et al. [2017] and understand their behavior.

For sinusoidal MLPs, Sitzmann et al. [2020] proposed an initialization scheme for stable training and convergence. Additionally, Paz et al. [2022] developed a multiresolution framework that controls the frequencies learned through initialization and data filtering.

Multiplicative filter networks (MFNs) Fathony et al. [2020] present an architecture that differs from MLPs by employing the Hadamard product instead of compositions. Building upon MFN, Bacon Lindell et al. [2022] shows how to control frequencies in the network and represent signals at multiple scales. However, as each representational atom in the network spans fewer frequencies, a sinusoidal MFN may require more parameters to represent the same amount of frequencies. Additionally, Bacon truncates the frequency spectrum of the signal, leading to ringing artifacts.

We propose to use sinusoidal INRs to represent periodic textures. We prove that if the first layer is initialized with weights compatible with a period P , then the network is also periodic with period P .

Regarding seamless textures, inspired by Pérez et al. [2003], we model it as a term in the loss function using a Poisson problem. This strategy has been explored in INRs for tasks such as compositing gradients Sitzmann et al. [2020] and face morphing Schardong et al. [2023]. SIREN trains the INR using only the gradients, leading to the learning of the signal up to an integral constant, which is problematic when we have multiple channels. In contrast, our training scheme incorporates both gradient and image values.

3 Periodic Neural Networks

For simplicity, along this section, we assume the image’s codomain to be \mathbb{R} , since the results can be easily extended to multiple channels.

A *periodic image* $\ell : \mathbb{R}^2 \rightarrow \mathbb{R}$ is a function satisfying the property $\ell(x) = \ell(x + P)$ with $P = (P_1, P_2) \in \mathbb{R}^2$ giving the *periods* along the axes x_1 and x_2 . For an example, consider the *harmonic* $h(x_1, x_2) = a \sin(x_1\omega_1 + x_2\omega_2 + \varphi)$ where $\omega_i = k_i \frac{2\pi}{P_i}$, with $k_i \in \mathbb{Z}$, are the *frequencies*, a is the *amplitude*, and φ is the *phase shift*. Such functions play a central role in *Fourier series*, where the periodic function ℓ can be approximated by a sum of harmonic functions.

3.1 Shallow Sinusoidal networks

Observe that summing harmonic functions also results in a *sinusoidal network* $f : \mathbb{R}^2 \rightarrow \mathbb{R}$ with a single layer:

$$f(x) = L \circ s(x) = c_0 + \sum_{i=1}^n c_i \sin(\omega_i x + \varphi_i) \quad (1)$$

where the *first* layer $s : \mathbb{R}^2 \rightarrow \mathbb{R}^n$ projects the input coordinates $x = (x_1, x_2)$ into a list of harmonics:

$$s(x) = \sin(\omega x + \varphi) = \begin{pmatrix} \sin(\omega_1 x + \varphi_1) \\ \vdots \\ \sin(\omega_n x + \varphi_n) \end{pmatrix}. \quad (2)$$

Where $\omega_i x = \omega_{i1}x_1 + \omega_{i2}x_2$. Thus, the matrix $(\omega_1, \dots, \omega_n)$ gives the *frequencies* and $(\varphi_1, \dots, \varphi_n)$ the *phase shifts*. The *linear* layer L combines the harmonics with the *amplitudes* c_i and adds a bias c_0 .

For the network f to be periodic with periods (P_1, P_2) we can simply choose $\omega_{ij} = k_{ij} \frac{2\pi}{P_i}$, with k_{ij} being integers. Section 3.4 presents an initialization of k_{ij} using ideas from Fourier series.

3.2 Deep sinusoidal networks

We compose the first layer of f with a hidden layer $h : \mathbb{R}^n \rightarrow \mathbb{R}^m$ to make f deeper. That is, $f = L \circ h \circ s$, with $h \circ s(x) := \sin(W \cdot s(x) + b)$, where $W \in \mathbb{R}^{m \times n}$ is the *hidden matrix*, and $b \in \mathbb{R}^m$ is the *bias*.

The i th coordinate of h one express as a *sinusoidal perceptron*:

$$h_i \circ s(x) = \sin \left(\sum_{j=1}^n W_{ij} \sin(\omega_j x + \varphi_j) + b_i \right).$$

Thus, f consists of multiple sine compositions. In a more general sense, a *sinusoidal network* is a function constructed by combining sinusoidal perceptrons. Furthermore, by adding more hidden layers to f , we obtain a sinusoidal *multilayer perceptron* (MLP). Training such networks can be challenging because using the sine as an activation function may lead to instability in deep architectures Parascandolo et al. [2017]. Sitzmann et al. [2020] overcome this by proposing SIREN, which gives a special initialization scheme for sinusoidal MLPs, providing stability during training. Clearly, the activation function is periodic, but the network f may not. Recall that even summing periodic function may result in non-periodic function: e.g. $\sin(x) + \sin(\sqrt{2}x)$. Furthermore, to accurately represent a periodic function, we must have control over the network’s period.

In this work, we observe that by initializing the first layer s of a sinusoidal MLP f with integer frequencies, specifically $\omega_{ij} = k_{ij} \frac{2\pi}{P_i}$ where $k_{ij} \in \mathbb{Z}$, we can prove that f will be periodic with period $P = (P_1, P_2)$. In other words, $f(x_1, x_2) = f(x_1 + P_1, x_2 + P_2)$.

For simplicity, let f be a 1D function, i.e. $f : \mathbb{R} \rightarrow \mathbb{R}$, the general case follows analogously. Assuming the first layer to be periodic with period P , we see that its frequencies are expressed as $\omega_j = k_j \frac{2\pi}{P}$. Moreover, observe that if we

prove that if each sinusoidal neuron $h(x) = \sin(\sum_{i=1}^n a_i \sin(\omega_i x + \varphi_i))$ expands as a sum of harmonics with period P , then, the output of h is periodic with period P . The proof of this fact follows from the following identity Novello [2022]:

$$h(x) = \sum_{\mathbf{l} \in \mathbb{Z}^n} \left[\prod_{i=1}^n J_{l_i}(a_i) \right] \sin(\mathbf{l}\omega x + \varphi + b). \quad (3)$$

Since each frequency in this sum is written as $\mathbf{l}\omega = \frac{2\pi}{P} \mathbf{l}\mathbf{k}$, we have that h is periodic with period P . We note that an expansion similar to Equation 3 was also presented in Yüce et al. [2022].

For sinusoidal MLP with two hidden layers, we truncate the expansion given by the expansion of the first layer. Thus the input of the second hidden layer is a finite sum of sines and Equation 3 can be applied. For the truncation, we use the fact that the amplitudes $\prod_{i=1}^n J_{l_i}(a_i)$ goes rapidly to zero as $\|\mathbf{l}\|_\infty$ increases. This is due to the following inequality Novello [2022]:

$$\left| \prod_{i=1}^n J_{l_i}(a_i) \right| < \prod_{i=1}^n \frac{\left(\frac{|a_i|}{2}\right)^{\|l_i\|}}{|l_i|!}. \quad (4)$$

Applying induction in the above procedure implies the result:

Theorem 1 *If the first layer of a sinusoidal MLP f is periodic with period P , then f is also periodic with period P .*

Theorem 1 allows us to use sinusoidal MLPs to represent periodic functions. We define a *periodic INR* to be a sinusoidal MLP such that its first layer is periodic.

3.3 Multiresolution sinusoidal networks

To represent textures using INRs we need to represent them in multiresolution. For this, we adopt the *multiresolution network* (MRnet) Paz et al. [2022] as a representation. Here, a MRnet is a network $f: \mathbb{R}^2 \times [0, N] \rightarrow \mathbb{R}$ defined as a sum of N periodic INR $g_i: \mathbb{R}^2 \rightarrow \mathbb{R}$:

$$f(x, t) = c_0(t)g_0(x) + \dots + c_{N-1}(t)g_{N-1}(x), \quad (5)$$

The contribution of each *stage* g_i in Equation 5 is controlled by $c_i(t) = \max\{0, \min\{1, t - i\}\}$. This allows us to navigate in the multiresolution using a parameter $t = k + \delta$ with $k \in \mathbb{N}$ and $0 \leq \delta \leq 1$:

$$f(x, t) = g_0(x) + \dots + g_k(x) + \delta g_{k+1}(x). \quad (6)$$

The *level of details* $f(\cdot, t)$ evolve continuously. We set the first layer of each periodic INR g_i with integer frequencies, since Theorem 1 says that in this case f will *periodic* with respect to x .

3.4 Frequency initialization

The first layer of a sinusoidal INR projects the input coordinates into a list of sines (Eq. 2). Next, we show that in a shallow network, this gives the frequencies of the signal represented by a Fourier series. Thus, the initialization of the first layer is important for network performance. Following the conclusions of Theorem 1, we define the first layer's frequencies to be integer multiples of a period.

Let $\ell: \mathbb{R}^2 \rightarrow \mathbb{R}$ be a periodic image (the *ground-truth*) with period P and $f: \mathbb{R}^2 \rightarrow \mathbb{R}$ be a periodic INR. To define the integer matrix k_{jl} of the first layer of f we follow ideas from Fourier series. If $\ell \in L^1(P)$, the *Fourier theorem* says that it expands in a series:

$$\ell(x) = \sum_{\mathbf{k} \in \mathbb{Z}^2} c_{\mathbf{k}} e^{i\omega_{\mathbf{k}} x}, \quad (7)$$

where $c_{\mathbf{k}}$ are the *Fourier coefficients*, and $\omega_{\mathbf{k}} = 2\pi \left(\frac{k_1}{P_1}, \frac{k_2}{P_2}\right)$ with $\mathbf{k} = (k_1, k_2)$. In practice, we truncate the Fourier series summing over the integers $\mathbf{k} \in [-B, B]^2$, where B is a *bandlimit*.

On the other hand, assuming f to be a network with a single layer (Eq (1)) and adding $\frac{\pi}{2}$ to the biases, we obtain:

$$f(x) = \frac{a_0}{2} + \sum_{k=1}^n a_k \cos(\omega_k x + \varphi_k) \quad (8)$$

$$= c_0 + \sum_{k=1}^n c_k e^{i\omega_k x} + \sum_{k=-n}^{-1} c_k e^{i-\omega_{|k|} x}, \quad (9)$$

where $c_k = \frac{a|k|}{2} e^{\text{sign}(k)i\varphi_{|k|}}$ with $\varphi_0 = 0$, and $\omega_j = 2\pi \left(\frac{k_{j,1}}{P_1}, \frac{k_{j,2}}{P_2} \right)$. Thus, for f to approximate the truncated series in Eq. (7), we can set the integers k_j in a set $\mathbf{K} \subset [-B, B]^n$ such that $-\mathbf{K} = [-B, B]^n \setminus \mathbf{K}$.

When f contains hidden layers, we initialize its parameters following the scheme in Sitzmann et al. [2020]. Notice that we initialized f with a finite number of frequencies in the frequency set \mathbf{K} . However, the layer composition produces many other frequencies as the depth of the network increases. Equation 3 justifies this claim.

Regarding the frequency initialization of each stage g_i , we split the frequency set \mathbf{K} in N subsets \mathbf{K}_i sorted by length. Thus, the first layer of g_i is initialized with the frequencies in \mathbf{K}_i . This initializes subsequent stages using only frequencies that were not chosen in previous stages enforcing the early stages to contain the lower frequencies, then as stages advance we add the higher frequencies.

3.5 Network training

Let $\ell : \Omega \subset \mathbb{R}^2 \rightarrow \mathcal{C}$ be an image (*ground-truth*) defined in the rectangular domain $\Omega = [0, P_1] \times [0, P_2]$. We aim to approximate ℓ by a periodic INR $f : \mathbb{R}^2 \rightarrow \mathcal{C}$ with periods (P_1, P_2) such that the resulting image is seamless. For this, define the weights ω_{ij} of the first layer of f in the form $k_{ij} \frac{2\pi}{P_i}$ with $k_{ij} \in \mathbb{Z}^2$. Again, this implies that the first layer is periodic with periods (P_1, P_2) , then, Theorem 1 implies that f is also periodic with the same periods. To force the resulting texture to be seamless at the boundary $\partial\Omega$ of Ω , we design a loss function based on a *Poisson problem*.

Specifically, we use the Jacobian $\mathbf{J}(\ell)$ of ℓ to train the periodic INR f . For this, we define a matrix field U such that its primitive approximates a seamless tileable texture at $\partial\Omega$. Then we enforce $\ell = f$ at some region of Ω . This can be modeled using:

$$\min \int_{\Omega} \lambda \|\mathbf{J}(f) - U\|^2 dx \text{ subject to } (1 - \lambda)(\ell - f) = 0 \text{ in } \Omega. \quad (10)$$

Where $\lambda : \Omega \rightarrow [0, 1]$ is a weight function indicating that U should match the Jacobian of f if it is close to one ($\lambda \approx 1$), and enforces $\ell = f$, otherwise. We propose to use this variational problem to define the following loss function to train the parameters θ of f .

$$\mathcal{L}(\theta) = \int_{\Omega} \lambda \|\mathbf{J}(f) - U\|^2 dx + \int_{\Omega} (1 - \lambda)(\ell - f)^2 dx. \quad (11)$$

Thus, \mathcal{L} trains f to *seamless clone* the primitive of U to f in Ω . Unlike classical approaches that rely on pixel manipulation, seamless cloning operates on the image gradients. Note that λ depends on the position x . In practice, we consider it to have high values near $\partial\Omega$. As a result, the training forces the matching of the Jacobian of f with U near $\partial\Omega$. In fact, since f is periodic, we are training it on the torus given by the identification of the opposite edges of Ω . Classical methods do not provide such flexibility.

4 Experiments

This section presents experiments using our method for tileable material texture representation. We begin by fitting a tileable pattern across multiple scales, and assess its performance qualitatively. Then, we train the network using a sample containing repetitions of the pattern, with a fundamental period smaller than the training domain. For this, we utilize masks to exclude certain parts of the image during training and examine the network’s ability to reconstruct them. Additionally, we address non-tileable patterns that can be made seamless using Poisson regularization. Finally, we provide comparative evaluations with related methods.

4.1 Seamless Tileable Materials

We start with a single tile, matching the fundamental period of a texture, with a resolution of 1024^2 pixels and 8 bits per color channel in RGB space. We convert the image to YCbCr and train a MRnet, using the framework in Paz et al. [2022], consisting of a 6 periodic INRs (stages). We use periodic INRs with a single hidden layer, and heterogeneous width, as experiments indicated that we need fewer parameters to fit an image of lower resolution and low-frequency details. The initialization uses the scheme described in Sec 3.4. The architecture of the hidden layer (number of input/output neurons) and the band limits of the first layer are in Table 4.1.

Figure 1 presents a qualitative comparison between the original image and the reconstructed image using our method. Observe that the images exhibit a high degree of similarity with a PSNR of 31.8 dB. Additionally, our model achieves this level of fidelity using 855,572 parameters, which is less than the number of pixels in the image (1,048,576).

Stage	Band-Limit	Hidden Input	Hidden Output
0	$[0, 3] \times [-3, 3]$	24	32
1	$[0, 6] \times [-6, 6]$	48	32
2	$[0, 12] \times [-12, 12]$	80	64
3	$[0, 24] \times [-24, 24]$	192	160
4	$[0, 56] \times [-56, 56]$	384	256
5	$[0, 128] \times [-128, 128]$	1024	512

Table 1: M-Net architecture.

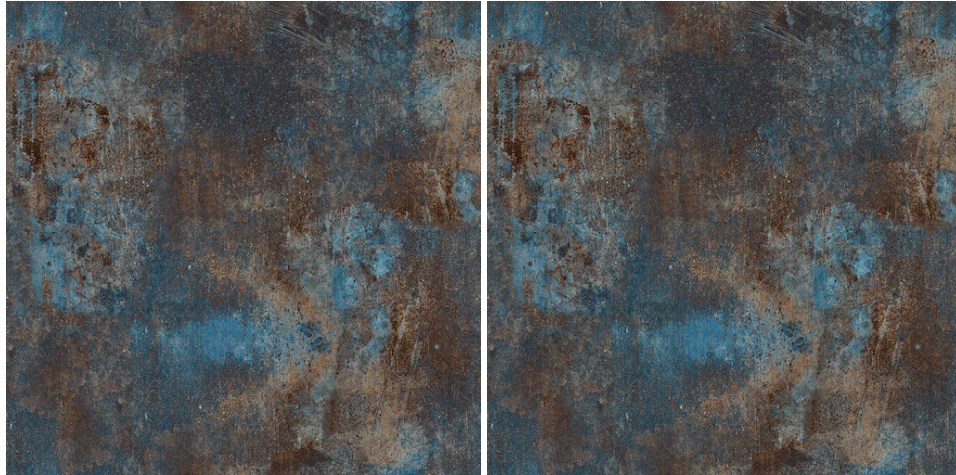


Figure 1: Original image (left); reconstruction of the network (right)

Our model also demonstrated the ability to encode information at multiresolution giving an even better compression compared to a traditional Mipmap.

To verify the periodicity of our INR model (Secs 3.2 and 3.3), we evaluate the network in a larger domain $([-2, 2]^2)$ than its training domain $[-1, 1]^2$; Figure 2 illustrates it for levels of detail 2, 4, and 6.

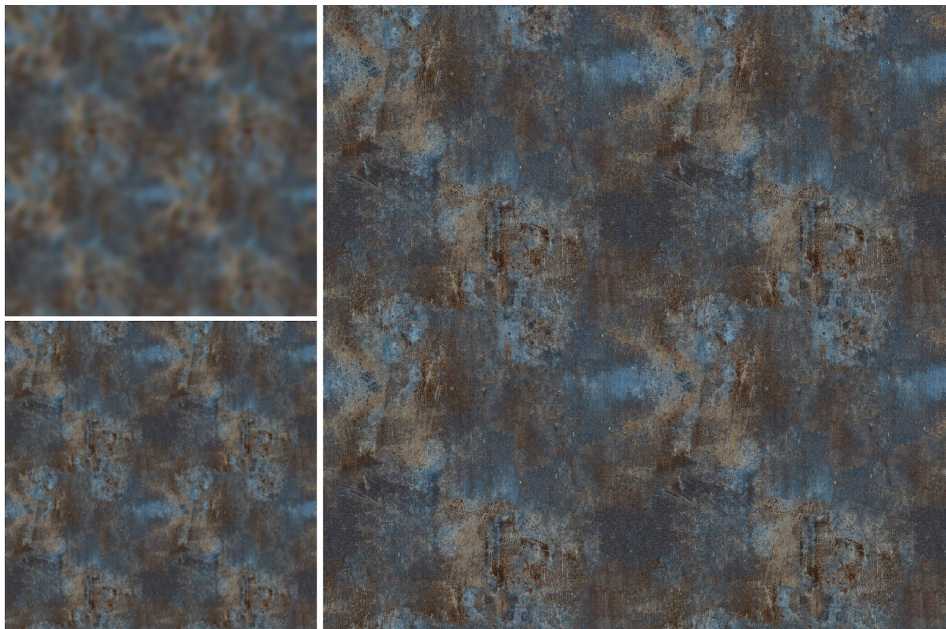


Figure 2: Reconstructed multiresolution levels extrapolation. Top left: level 2; bottom left: level 4; right: level 6.

4.2 Repeating Patterns in Sample

We can also represent a texture with a fundamental period smaller than the sample size. This means that the periodic pattern repeats multiple times within the sample. To address this, we can specify the fundamental period either by prior knowledge or through pre-processing of the image, and train the network using the entire data or only a specific portion of it.

Figure 3 showcases a texture sample where the pattern is repeated twice, and its extrapolated reconstructions in the region $[0, 3]^2$. The training considered $[-1, 1]^2$, with a specified period of 1. Figures 3 (a) and (c) show the training data, while the network reconstruction is given by (b) and (d), respectively. In (a-b), all coordinates within the region are provided, thus the network learns a periodic representation of the pattern. In (c-d), we employ a mask to exclude a small part while preserving a contiguous region that contains the fundamental period. Again, our method reconstructs the periodic pattern across the entire region. This demonstrates that the over-determined problem does not negatively impact the results.

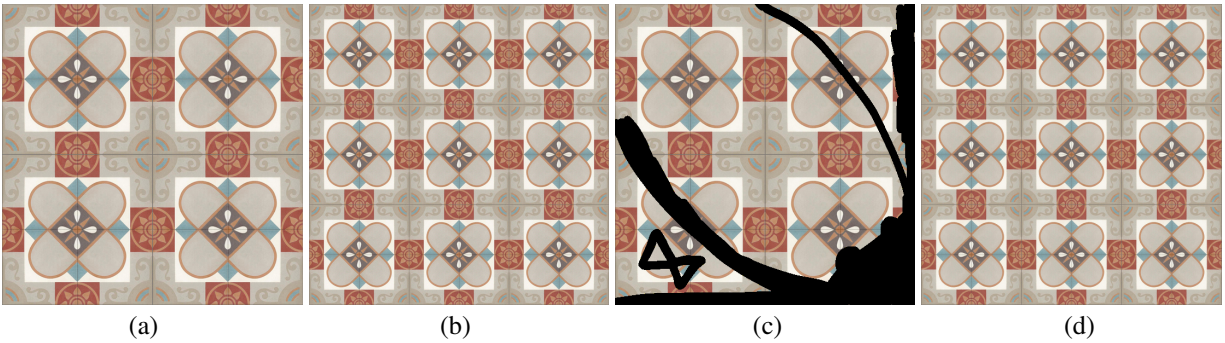


Figure 3: (a) Full training data. (b) Network reconstruction from full data. (c) Masked training data; black pixels were not provided in training. (d) Network reconstruction from masked data.

In the next experiment, a few points have no correspondents visible in any of the periods. This generates an artifact that is noticed across all occurrences of that pattern (Figure 4).

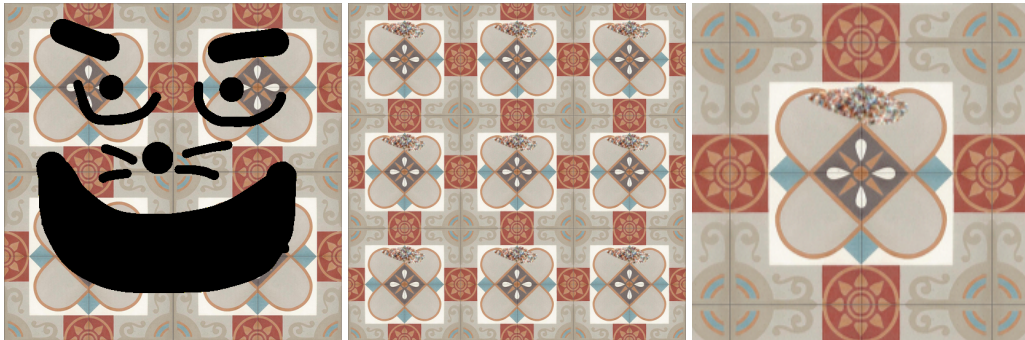


Figure 4: From left to right: training data, network reconstruction in $[0, 3]^2$, and zoom in one tile to highlight the reconstruction artifact.

Next, we selectively remove points from the training data encouraging a sparse representation of the pattern. We generate the mask by randomly selecting a pixel and subsequently discarding all pixels that correspond to the selected one based on the pattern’s period. Consequently, the mask encompasses exactly $1/4$ of the total pixels. Figure 5 shows the training data, where the black pixels were removed from training, and the learned texture in $[2, 6]^2$.

Even in this case, our method captures the underlying periodicity. This provides evidence that we can use the training data at any part of the domain. In other words, we only need a single sample from the class of equivalence defined by the periodicity to reconstruct the image without requiring any additional regularization.



Figure 5: On the left, the masked input data, where the black pixels were removed from training. On the right, the network reconstruction.

4.3 Seamless with Poisson Regularization

When obtaining a sample for a material, the inherent irregularity in the sample’s pattern poses a challenge in seamlessly stitching it together. Achieving a seamless material is crucial for numerous applications. This section details the application of our methodology to generate seamless results from material patches.

We train a periodic INR for this task using the loss function of Section 3.5 which is based on the Poisson equation. In regard to classical Poisson problem solutions, a key observation of our method is the inversion of boundary and interior conditions. We employ masks (the function λ in Eq 11) to delineate the supervision of gradients at the border, while color values are supervised within the interior of the region. Given that our work is situated in the realm of periodic functions, the problem domain is equivalently represented as a torus, thus obviating traditional boundaries.

While binary masks can produce satisfactory outcomes, they often introduce artifacts at the gradient of the reconstructed network (Figure 6), requiring customized adjusts, per image, of the weights of the loss function components. Consequently, we opted for soft masks computed via a distance function to the center of the mask. In our experiments, we utilized the L_2 distance, but any L_p distance can be employed as a parameter for refining the results.

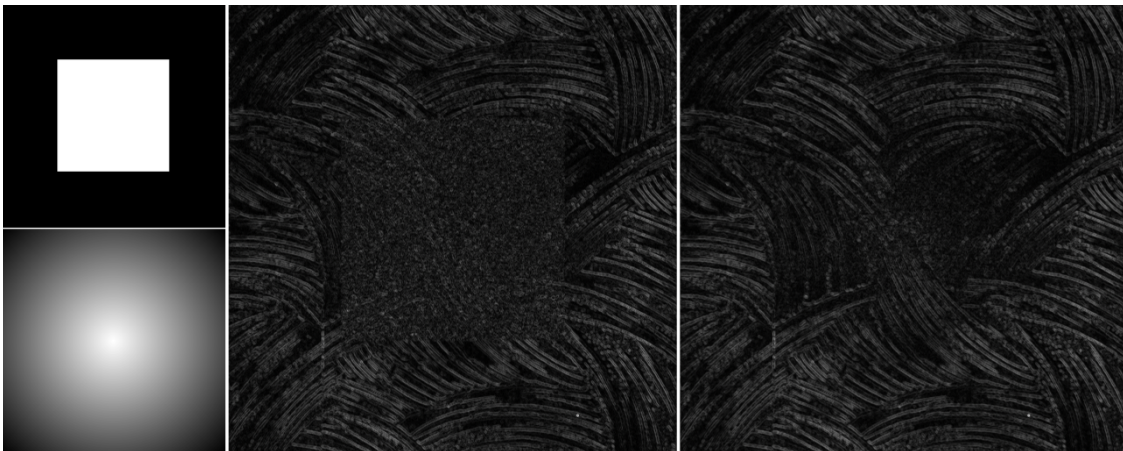


Figure 6: Binary mask (top), soft mask (bottom), and the normalized magnitude of the gradients of the trained networks. This is the gradient of the texture in Line 2 of Fig 7.

Figure 7 illustrates several seamless reconstructions (second column) of non-tileable material samples (first column). The first line shows an example of a fabric patch containing only fine details. The second line gives the case of a pattern featuring medium geometric details. Meanwhile, the third line presents the reconstruction of a pattern characterized by larger details. Note that in all instances, our method adeptly conceals seams through the uniformization of photometric discrepancies. This results in a visually cohesive representation that effectively camouflages the transitions between material patches.

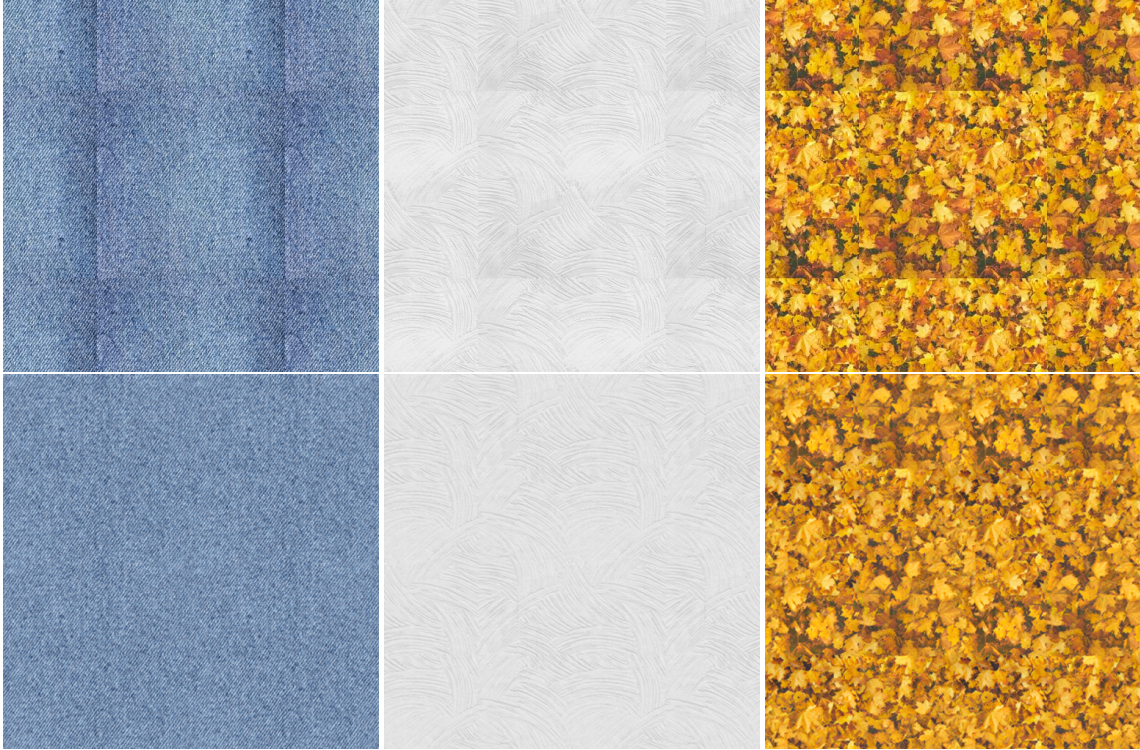


Figure 7: Seamless reconstruction of jeans fabric (only fine details) on the left. Seamless reconstruction of a patch of a wall (medium details) on the middle; note that although this texture looks homogeneous it has fine details as can be seen on its gradient in Fig 6. Finally, the third column gives the reconstruction of the leaves textures containing big details.

4.4 Comparisons

While SIREN and MRnet employ periodic activation functions, this is insufficient for learning periodic images with supervision in a restricted domain. Figure 8 shows a comparison between image reconstruction/extrapolation using SIREN and our periodic model.

For this, we use an identical architecture to SIREN: periodic INR with 3 hidden layers, of the form $\mathbb{R}^{256} \rightarrow \mathbb{R}^{256}$. The key difference lies in the initialization: we randomly selected 256 pairs of integer frequencies from the range $[0, 30] \times [-30, 30]$, whereas SIREN follows the initialization given in Sitzmann et al. [2020] with $\omega_0 = 30$. The images were trained on a 512×512 grid within the region $[-1, 1]$ for 500 epochs. The extrapolations are displayed in $[-2, 2]$.

It is worth noting that beyond the domain of supervision, the SIREN’s reconstruction is very noisy, while our approach captures the underlying periodic pattern.

We also applied the Poisson regularization, using binary masks, to reconstruct non-tileable patterns in a seamless way using both SIREN and our periodic initialization, see Figure 9. Again, SIREN’s reconstruction displays only noise outside the supervised domain, while our periodic initialization reconstructs a seamless texture.

To reconstruct seamless tiles using Poisson equation, Pérez et al. [2003] suggests to manipulate the pixels intensities at the borders so that left = right and top = bottom, which can be achieved by averaging these values. These intensities should be given as boundary conditions while the gradients should be given at all other positions. In Figure 10, we compare this strategy with the one presented in Section 4.3. Note that our approach gives a more uniform result, better reducing the photometric differences present in the pattern.

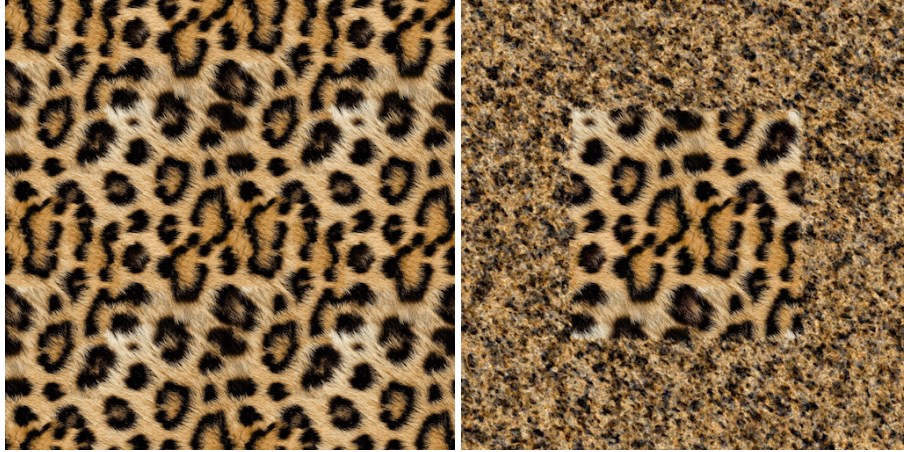


Figure 8: Comparing our method (left) with Siren (right) on extrapolation.

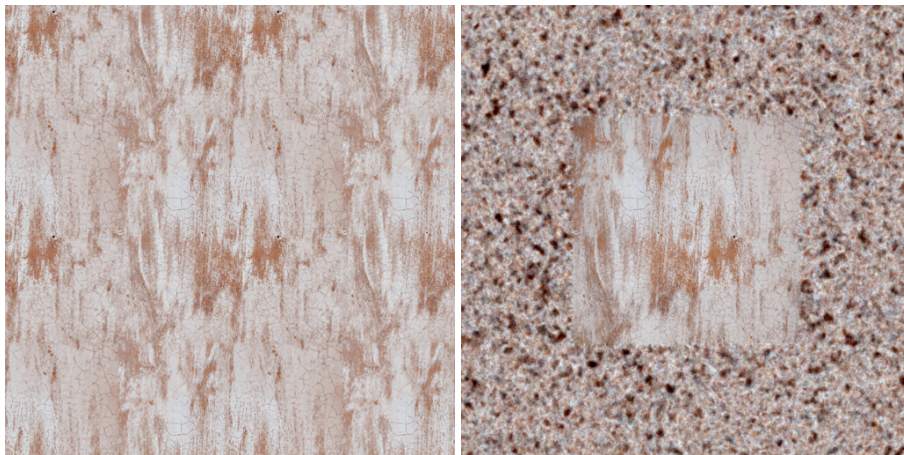


Figure 9: Non-tileable patten. Our periodic initialization vs Siren's.

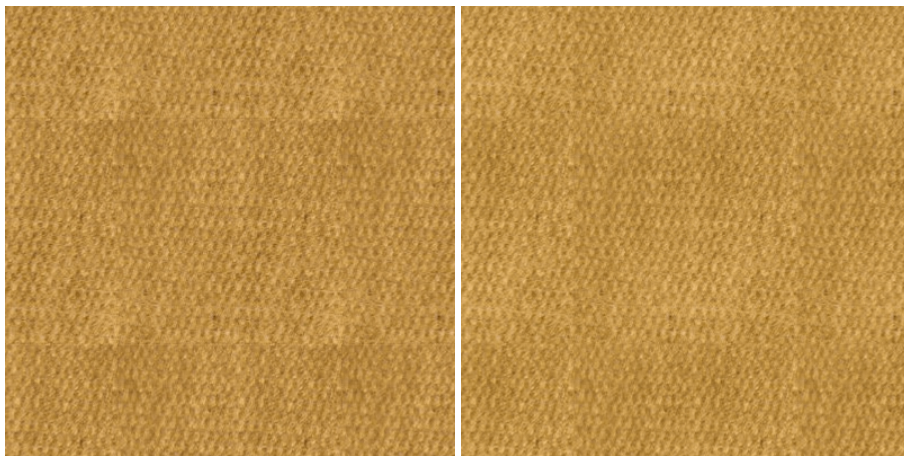


Figure 10: Average border (left). Gradient Border (right).

5 Applications

Paz et al. [2022] have demonstrated MRNet capabilities of encoding mip-mapping and displaying an anti-aliased version of an image, adapted to the required resolution. This section demonstrates practical applications of this property in mapping textures to surfaces.

5.1 Surface Texture Mapping

We present a simple renderer to show the application of our networks in surface texture mapping (Fig.11). We directly evaluate the network at the uv -coordinates of each fragment in a rendering pipeline. First, we map the uv -coordinates from the range $[0, 1]$ to $[-1, 1]$; then, for the torus, we apply a factor of 2 in the u coordinate for a better aspect to the rendering. We can also scale the coordinates so that it spans multiple periods of the texture.



Figure 11: Neural texture mapping on the torus using its uv -coordinates. Line 1 shows four texture examples. Line 2 presents these textures affected by different torus transformations.

Note that as our network is continuous in space and encodes levels of details, we can evaluate it in any coordinates, and interpolate between levels, akin to Mip-Map Williams [1983]. In this regard, we can perform anti-aliasing similarly to the results in Paz et al. [2023].

6 Conclusion and Future Work

We presented an unified framework for modeling seamless textures by incorporating Fourier series ideas into neural network architectures. Our approach demonstrates the ability to train the network using partial texture data, making it more compact, and capturing sharper details compared to the ground truth in certain cases.

While we have made significant progress in understanding the impact of sinusoidal network initialization on representation capacity, there are still paths for future exploration. Although we have constrained the space of frequency choices by selecting integer multiples of a period and partitioning the frequency space, determining the appropriate band limit remains an empirical task. In our current approach, we freeze the weights of the first layer to maintain their constancy throughout training. However, finding a way to make these weights learnable parameters while preserving the desired period is a valuable research direction.

Extending our approach to higher dimensions is a direction for future work. Additionally, exploring the application of our method to represent other graphical objects, such as hypertextures, Perlin and Hoffert [1989], by leveraging the versatility of vector fields in combination with surface representations, holds great potential.

To fully integrate neural networks as primitives in a graphics pipeline, it is crucial to develop methods for operating and editing them. The functional structure of sinusoidal INRs provides opportunities to explore algebraic structures for network manipulation.

Periodic INRs have high-capacity representation. When restricted to periodic functions domain, they can naturally compress the images, specially in multiresolution. However, investigating compression techniques tailored for sinusoidal networks is essential for achieving compact storage and efficient transmission over computer networks. Exploring the distribution of signal frequencies to inform network initialization is a promising direction in this regard.

References

- Vincent Sitzmann, Julien N.P. Martel, Alexander W. Bergman, David B. Lindell, and Gordon Wetzstein. Implicit neural representations with periodic activation functions. In *Proc. NeurIPS*, 2020.
- Tiago Novello. Understanding sinusoidal neural networks. *arXiv preprint arXiv:2212.01833*, 2022.
- Gizem Yüce, Guillermo Ortiz-Jiménez, Beril Besbinar, and Pascal Frossard. A structured dictionary perspective on implicit neural representations. In *Proceedings of the IEEE/CVF Conference on Computer Vision and Pattern Recognition*, pages 19228–19238, 2022.
- Patrick Pérez, Michel Gangnet, and Andrew Blake. Poisson image editing. In *Seminal Graphics Papers: Pushing the Boundaries, Volume 2*, pages 577–582. 2003.
- Harrison Paz, Daniel Perazzo, Tiago Novello, Guilherme Schardong, Luiz Schirmer, Vinicius da Silva, Daniel Yukimura, Fabio Chagas, Helio Lopes, and Luiz Velho. Mr-net: Multiresolution sinusoidal neural networks. *Computers & Graphics*, 2023.
- Adobe. Substance 3d sampler, 2023. <https://www.adobe.com/products/substance3d-sampler.html> [Accessed: Jan 2024].
- James F. Blinn and Martin E. Newell. Texture and reflection in computer generated images. *Commun. ACM*, 19(10): 542–547, oct 1976. ISSN 0001-0782. doi:10.1145/360349.360353. URL <https://doi.org/10.1145/360349.360353>.
- Ken Perlin. An image synthesizer. *SIGGRAPH Comput. Graph.*, 19(3):287–296, jul 1985. ISSN 0097-8930. doi:10.1145/325165.325247. URL <https://doi.org/10.1145/325165.325247>.
- A.A. Efros and T.K. Leung. Texture synthesis by non-parametric sampling. In *Proceedings of the Seventh IEEE International Conference on Computer Vision*, volume 2, pages 1033–1038 vol.2, 1999. doi:10.1109/ICCV.1999.790383.
- Paul Haeberli. Paint by numbers: Abstract image representations. In *Proceedings of the 17th Annual Conference on Computer Graphics and Interactive Techniques, SIGGRAPH '90*, page 207–214, New York, NY, USA, 1990. Association for Computing Machinery. ISBN 0897913442. doi:10.1145/97879.97902. URL <https://doi.org/10.1145/97879.97902>.
- Li-Yi Wie, Sylvain Lefebvre, Vivek Kwatra, and Greg Turk. State of the Art in Example-based Texture Synthesis. In M. Pauly and G. Greiner, editors, *Eurographics 2009 - State of the Art Reports*. The Eurographics Association, 2009.
- A. Lagae, S. Lefebvre, R. Cook, T. DeRose, G. Drettakis, D.S. Ebert, J.P. Lewis, K. Perlin, and M. Zwicker. A survey of procedural noise functions. *Computer Graphics Forum*, 29(8):2579–2600, 2010. doi:<https://doi.org/10.1111/j.1467-8659.2010.01827.x>. URL <https://onlinelibrary.wiley.com/doi/abs/10.1111/j.1467-8659.2010.01827.x>.
- Cem Yuksel, Sylvain Lefebvre, and Marco Tarini. Rethinking Texture Mapping. *Computer Graphics Forum*, 2019. ISSN 1467-8659. doi:10.1111/cgf.13656.
- Robert Jagnow, Julie Dorsey, and Holly Rushmeier. Stereological techniques for solid textures. *ACM Trans. Graph.*, 23(3):329–335, aug 2004. ISSN 0730-0301. doi:10.1145/1015706.1015724. URL <https://doi.org/10.1145/1015706.1015724>.
- Ares Lagae, Craig S. Kaplan, Chi-Wing Fu, Victor Ostromoukhov, and Oliver Deussen. Tile-based methods for interactive applications. In *ACM SIGGRAPH 2008 Classes, SIGGRAPH '08*, New York, NY, USA, 2008. Association for Computing Machinery. ISBN 9781450378451. doi:10.1145/1401132.1401254. URL <https://doi.org/10.1145/1401132.1401254>.

- Li-Yi Wei. Tile-based texture mapping on graphics hardware. In *Proceedings of the ACM SIGGRAPH/EUROGRAPHICS Conference on Graphics Hardware*, HWWS '04, page 55–63, New York, NY, USA, 2004. Association for Computing Machinery. ISBN 3905673150. doi:10.1145/1058129.1058138. URL <https://doi.org/10.1145/1058129.1058138>.
- J. Moritz, Stuart James, Tom S. F. Haines, Tobias Ritschel, and Tim Weyrich. Texture stationarization: Turning photos into tileable textures. *Computer Graphics Forum (Proc. Eurographics)*, 36(2):177–188, May 2017.
- Chandrajit Bajaj, Insung Ihm, and Sanghun Park. Compression-based 3d texture mapping for real-time rendering. *Graphical Models*, 62(6):391–410, 2000. ISSN 1524-0703. doi:<https://doi.org/10.1006/gmod.2000.0532>. URL <https://www.sciencedirect.com/science/article/pii/S1524070300905320>.
- J. Gutierrez, J. Rabin, B. Galerne, and T. Hurtut. On demand solid texture synthesis using deep 3d networks. *Computer Graphics Forum*, 39(1):511–530, nov 2019.
- Vasilis Toulatzis and Ioannis Fudos. Deep tiling: Texture tile synthesis using a constant space deep learning approach. In *Advances in Visual Computing: 16th International Symposium, ISVC 2021, Virtual Event, October 4-6, 2021, Proceedings, Part I*, page 414–426, Berlin, Heidelberg, 2021. Springer-Verlag. ISBN 978-3-030-90438-8. doi:10.1007/978-3-030-90439-5_33. URL https://doi.org/10.1007/978-3-030-90439-5_33.
- Xilong Zhou, Miloš Hašan, Valentin Deschaintre, Paul Guerrero, Kalyan Sunkavalli, and Nima Kalantari. Tilegen: Tileable, controllable material generation and capture, 2022.
- Karthik Vaidyanathan, Marco Salvi, Bartłomiej Wronski, Tomas Akenine-Möller, Pontus Ebelin, and Aaron Lefohn. Random-Access Neural Compression of Material Textures. In *Proceedings of SIGGRAPH*, 2023.
- Liang Shi, Beichen Li, Miloš Hašan, Kalyan Sunkavalli, Tamy Boubekour, Radomir Mech, and Wojciech Matusik. Match: Differentiable material graphs for procedural material capture. *ACM Trans. Graph.*, 39(6), nov 2020. ISSN 0730-0301. doi:10.1145/3414685.3417781. URL <https://doi.org/10.1145/3414685.3417781>.
- Jeong Joon Park, Peter Florence, Julian Straub, Richard Newcombe, and Steven Lovegrove. Deepsdf: Learning continuous signed distance functions for shape representation. In *Proceedings of the IEEE/CVF conference on computer vision and pattern recognition*, pages 165–174, 2019.
- Lars Mescheder, Michael Oechsle, Michael Niemeyer, Sebastian Nowozin, and Andreas Geiger. Occupancy networks: Learning 3d reconstruction in function space. In *Proceedings IEEE Conf. on Computer Vision and Pattern Recognition (CVPR)*, 2019.
- Tiago Novello, Guilherme Schardong, Luiz Schirmer, Vinicius da Silva, Helio Lopes, and Luiz Velho. Exploring differential geometry in neural implicits. *Computers & Graphics*, 108:49–60, 2022.
- Tiago Novello, Vinicius Da Silva, Guilherme Schardong, Luiz Schirmer, Helio Lopes, and Luiz Velho. Neural implicit surface evolution. In *Proceedings of the IEEE/CVF International Conference on Computer Vision*, pages 14279–14289, 2023.
- Vinicius da Silva, Tiago Novello, Guilherme Schardong, Luiz Schirmer, Hélio Lopes, and Luiz Velho. Neural implicit mapping via nested neighborhoods. *arXiv:2201.09147*, 2022.
- Lior Yariv, Yoni Kasten, Dror Moran, Meirav Galun, Matan Atzmon, Basri Ronen, and Yaron Lipman. Multiview neural surface reconstruction by disentangling geometry and appearance. *Advances in Neural Information Processing Systems*, 33, 2020.
- Nasim Rahaman, Aristide Baratin, Devansh Arpit, Felix Dräxler, Min Lin, Fred A. Hamprecht, Yoshua Bengio, and Aaron C. Courville. On the spectral bias of neural networks. In *International Conference on Machine Learning*, 2018.
- Matthew Tancik, Pratul P. Srinivasan, Ben Mildenhall, Sara Fridovich-Keil, Nithin Raghavan, Utkarsh Singhal, Ravi Ramamoorthi, Jonathan T. Barron, and Ren Ng. Fourier features let networks learn high frequency functions in low dimensional domains. *NeurIPS*, 2020.
- G. Parascandolo, H. Huttunen, and T. Virtanen. Taming the waves: sine as activation function in deep neural networks. 2017.
- Harrison Paz, Tiago Novello, Vinicius Silva, Guilherme Schardong, Luiz Schirmer, Fabio Chagas, Helio Lopes, and Luiz Velho. Multiresolution neural networks for imaging. In *2022 35th SIBGRAPI Conference on Graphics, Patterns and Images (SIBGRAPI)*, volume 1, pages 174–179, 2022. doi:10.1109/SIBGRAPI55357.2022.9991765.
- Rizal Fathony, Anit Kumar Sahu, Devin Willmott, and J Zico Kolter. Multiplicative filter networks. In *International Conference on Learning Representations*, 2020.
- D. Lindell, D. Van Veen, J. Park, and G. Wetzstein. BACON: Band-limited coordinate networks for multiscale scene representation. In *Proceedings of CVPR*, 2022.

Guilherme Schardong, Tiago Novello, Daniel Perazzo, Hallison Paz, Iurii Medvedev, Luiz Velho, and Nuno Gonçalves. Neural implicit morphing of face images. *arXiv preprint arXiv:2308.13888*, 2023.

Lance Williams. Pyramidal parametrics. *SIGGRAPH Comput. Graph.*, 17(3):1–11, jul 1983. ISSN 0097-8930. doi:10.1145/964967.801126. URL <https://doi.org/10.1145/964967.801126>.

K. Perlin and E. M. Hoffert. Hypertexture. In *Proceedings of the 16th Annual Conference on Computer Graphics and Interactive Techniques*, SIGGRAPH '89, page 253–262, New York, NY, USA, 1989. Association for Computing Machinery. ISBN 0897913124. doi:10.1145/74333.74359. URL <https://doi.org/10.1145/74333.74359>.